JIPB Journal of Integrative Plant Biology

Research Article
https://doi.org/10.1111/jipb.13663

Pleistocene glaciation advances the cryptic speciation of *Stellera chamaejasme* L. in a major biodiversity hotspot

Santosh Kumar Rana[1,2], Hum Kala Rana[1], Jacob B. Landis[3,4], Tianhui Kuang[1], Juntong Chen[1], Hengchang Wang[5], Tao Deng[1]*, Charles C. Davis[6]* and Hang Sun[1]*

1. CAS Key Laboratory for Plant Diversity and Biogeography of East Asia, Kunming Institute of Botany, Chinese Academy of Sciences, Kunming 650201, China
2. Arkansas Biosciences Institute, Arkansas State University, Jonesboro, Arkansas 72401, USA
3. School of Integrative Plant Science, Section of Plant Biology and the L.H. Bailey Hortorium, Cornell University, Ithaca, New York 14853, USA
4. BTI Computational Biology Center, Boyce Thompson Institute, Ithaca, New York 14853, USA
5. CAS Key Laboratory of Plant Germplasm Enhancement and Specialty Agriculture, Chinese Academy of Sciences, Wuhan Botanical Garden, Wuhan 430074, China
6. Department of Organismic and Evolutionary Biology, Herbaria, Harvard University, Cambridge, Massachusetts 02138, USA
*Correspondences: Hang Sun (sunhang@mail.kib.ac.cn); Charles C. Davis (cdavis@oeb.harvard.edu); Tao Deng (dengtao@mail.kib.ac.cn, Prof. Sun is fully responsible for the distribution of all materials associated with this article)

Santosh Kumar Rana

Hang Sun

ABSTRACT

The mountains of Southwest China comprise a significant large mountain range and biodiversity hotspot imperiled by global climate change. The high species diversity in this mountain system has long been attributed to a complex set of factors, and recent large-scale macroevolutionary investigations have placed a broad timeline on plant diversification that stretches from 10 million years ago (Mya) to the present. Despite our increasing understanding of the temporal mode of speciation, finer-scale population-level investigations are lacking to better refine these temporal trends and illuminate the abiotic and biotic influences of cryptic speciation. This is largely due to the dearth of organismal sampling among closely related species and populations, spanning the incredible size and topological heterogeneity of this region. Our study dives into these evolutionary dynamics of speciation using genomic and eco-morphological data of *Stellera chamaejasme* L. We identified four previously unrecognized cryptic species having indistinct morphological traits and large metapopulation of evolving lineages, suggesting a more recent diversification (~2.67–0.90 Mya), largely influenced by Pleistocene glaciation and biotic factors. These factors likely influenced allopatric speciation and advocated cyclical warming–cooling episodes along elevational gradients during the Pleistocene. The study refines the evolutionary timeline to be much younger than previously implicated and raises the concern that projected future warming may influence the alpine species diversity, necessitating increased conservation efforts.

Keywords: cryptic speciation, glacial-interglacial, Hengduan Mountains, north-south migration, *Stellera chamaejasme*

Rana, S.K., Rana, H.K., Landis, J.B., Kuang, T., Chen, J., Wang, H., Deng, T., Davis, C.C., and Sun, H. (2024). Pleistocene glaciation advances the cryptic speciation of *Stellera chamaejasme* L. in a major biodiversity hotspot. J. Integr. Plant Biol. **00:** 1–14.

INTRODUCTION

The mountains of Southwest China (Hengduan Mountains (HM), some parts of Qinghai-Tibet Plateau (QTP) and part of the Eastern Himalayas), known for their rich biodiversity paralleling tropical rainforests, have consistently attracted attention in macroevolutionary research (Wen et al., 2014; Sun et al., 2017; Rahbek et al., 2019; Spicer et al.,

2020). While existing theories predominantly attribute diversification to Miocene geological and climatic changes (23.0–5.3 million years ago; Mya) (Figure 1A) (Xing and Ree, 2017; Chen et al., 2018; Ding et al., 2020), the crucial role of cryptic speciation—evolutionary divergence that occurs without obvious morphological changes (Fišer et al., 2018) is often overlooked. This oversight has left the more recent Pleistocene epoch (starting around 2.6 Mya) on biodiversity largely underexplored, leaving a significant gap in our comprehension of recent evolutionary mechanisms.

Earlier studies, leaning toward broader taxonomic groups, inadvertently neglected intricate genetic nuances in these mountains (Xing and Ree, 2017; Chen et al., 2019; Zhang et al., 2021b). Such oversight could misguide or lead to spurious or at least partial conclusions regarding the true diversification history in the region—namely imposing artificially older boundaries that restrict inferences about the historical timing of diversification (Ding et al., 2020). While Miocene events are acknowledged, we contend that more recent glaciations and biological factors, such as pollinator interactions, have driven diversification in the region. We spotlight the Pleistocene glaciation's underrated influence on recent species evolution (Table 1), notably through cryptic speciation, offering fresh perspectives on iconic speciation events that likely occurred prior to Pleistocene glaciation (Tu et al., 2010; Zhang et al., 2011a; Xu et al., 2019; Zhang et al., 2021b).

The recurring glaciations of the Pleistocene epoch significantly altered the environment of the HM. While geological phenomena like orogeny and monsoons have been well researched (Myers et al., 2000; Mittermeier et al., 2011; Farnsworth et al., 2019), we highlight the Pleistocene glaciations' pivotal role in evolutionary shifts (Figure 1B). The HM's unique geography, its north-south and east-west divides (Chen et al., 2018), combined with river capture events (Sun et al., 2022), likely drove speciation during this epoch.

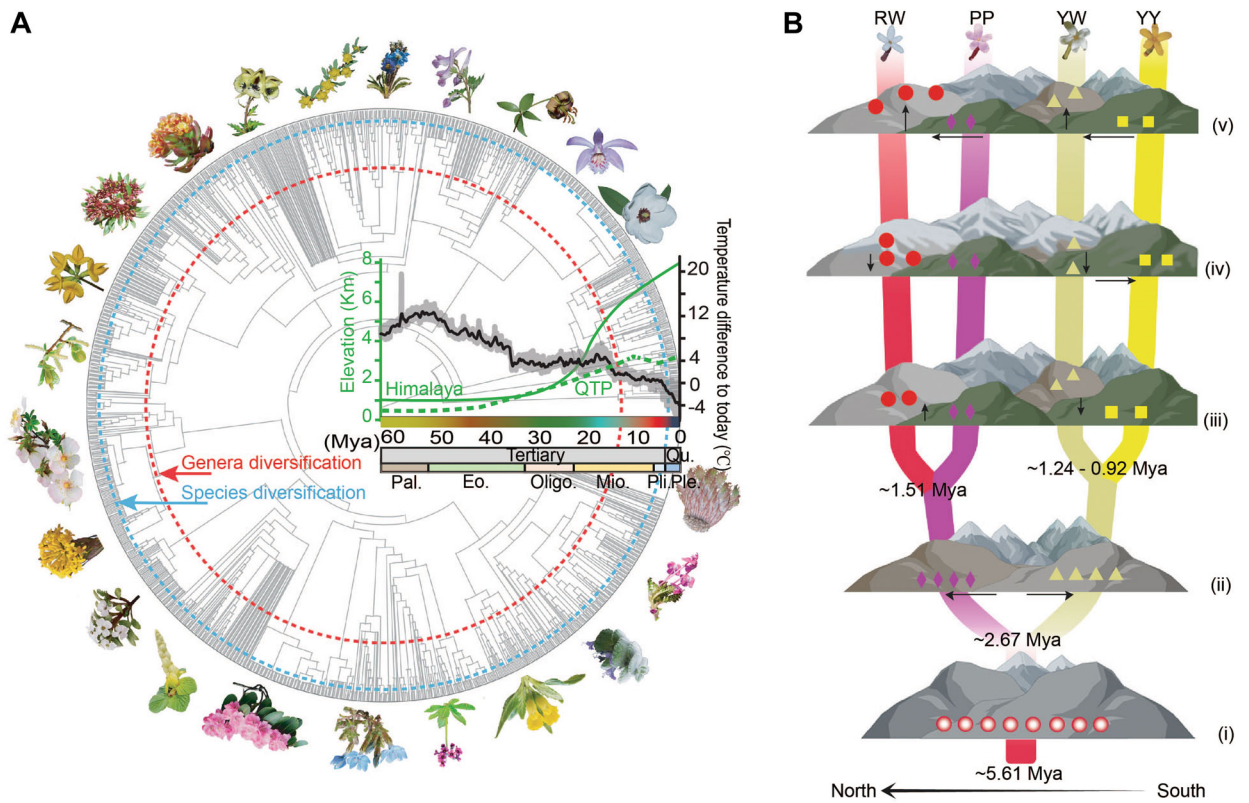

Figure 1. Theoretical framework for plant diversification and cryptic speciation in the mountain system

(A) The phylogenetic tree was constructed using v.PhyloMaker (Jin and Qian, 2019) with 1,520 vascular plant species (representative plant species provided at the edges of the tree) belonging to 235 genera and 56 families from the subnival zone of the Qinghai-Tibet Plateau (QTP) representing genera (red dotted line) and species (cyan dotted line) diversification (H. Sun, unpublished data). The global change in paleo-temperature (black line; modified from Westerhold et al. (2020)) and palaeo-elevation (green solid line for the Himalayas; modified from Spicer et al. (2020) and green dotted line for the QTP; modified from Zhao et al. (2022)) is embedded within the phylogenetic tree (phylogenetic tree not rooted with the geological time period; Pal.- Paleocene, Eo.- Eocene, Oligo.- Oligocene, Mio.- Miocene, Pli.- Pliocene, Ple.- Pleistocene). **(B)** Diagrammatic representation for the temporal dynamics of north-south and up-downslope migration model was overlaid within the molecular tree (tree not rooted) for the cryptic speciation of *Stellera chamaejasme*. The events are marked by numbers as (i) formation of *S. chamaejasme* at ~5.61 Mya, (ii) initial differentiation to form PP and YW ~ 2.67 Mya, (iii) differentiation to form four morphs–PP to RW ~ 1.51 Mya and YW to YY ~ 1.24–0.92 Mya, (iv) migration to the south and lowlands during glacial periods, (v) migration to the north and highlands during interglacial period. Each cryptic species morph is represented by a different shape color: PP, pink colored; RW, red colored; YW, light yellow colored; YY, yellow colored.

Table 1. Representative studies focused on cryptic diversity and speciation across the Hengduan Mountains (HM)

Study species	Species/ population	Divergence time (Mya)	Lineage/species diversification (Mya)
Pedicularis siphonantha complex (Liu et al., 2022)	Nine species + 12 *Pedicularis* species	6.04–10.38	2.48–5.30
Buddleja alternifolia Maxim. (Ma et al., 2021)	48 populations	2.91	1.15–1.48
Paeonia subsect. Delavayanae: Peonies (Zhao et al., 2021)	Two species (31 *P. delavayi* and 3 *P. ludlowii*)	10.93	NA
Roscoea tibetica Betalin (Li et al., 2021)	One species	15.40	NA
Yews (*Taxus wallichiana* Zucc.) (Liu et al., 2013)	43 populations of one species	4.20	2.10–2.40
White pine (*Pinus armandi* Franch.) (Liu et al., 2019)	One species + six outgroups species	9.58	4.39–7.36

Changes in "sky islands" (He and Jiang, 2014; Chen et al., 2019) and interactions, such as with pollinators and herbivores (Niu et al., 2021; Wessinger, 2021), further simulated the process of recent cryptic speciation (Eaton et al., 2012; Paudel et al., 2016).

For this study, we focus on *Stellera chamaejasme* L. (Thymelaceae), a species within the monotypic genus *Stellera* L. that serves as an ideal system to elucidate the complex dynamics of cryptic speciation catalyzed by Pleistocene glaciation. This species has a wide geographical range, diverse flower color morphs, ecological disparity, and distinct evolutionary trajectory (Figure 2) (Zhang et al., 2010). Despite the presence of four distinct color morphs in *S. chamaejasme*, the morphological distinctions between them remain indistinct, suggesting the possibility of cryptic speciation within what is conventionally considered a single species. Historically classified as two distinct species (Linnaeus, 1753; Léveillé, 1912) or two forms (Huang, 1985), *S. chamaejasme* is now broadly recognized as a single species with red-white and yellow flower morphs (Wang and Gilbert, 2007). The red-white flower variants, denoted the RW morphs (Figure 2B), consist of individuals with red calyx tubes and white lobes and are widely found from the QTP, HM to northeast China and Siberia. Conversely, the purely yellow flower type (hereafter referred to as YY morph; Figure 2E), exhibiting a yellow calyx tube and yellow lobes, is located from the southern region of the HM to the Yunnan-Guizhou Plateau (Figure 2A) (Huang, 1985). Additionally, we have observed a pure pink flower type (referred to as PP morph; Figure 2C), with pink calyx tubes and pink lobes, located in Yajiang county of the HM. Lastly, a yellow-white flower variant (denoted as YW morph; Figure 2D), having a yellow calyx tube and white lobes, is found in the central part of the HM.

Here, we aim to provide a window into the paradigm of diversification using the evolutionary histories of *S. chamaejasme* across different ecological regimes of the mountains of Southwest China. Specifically, this study aims to: (1) recalibrate our understanding of diversification mechanisms, highlighting the influential role of Pleistocene glaciation and ecological dynamics; and (2) examine the evolutionary histories of *S. chamaejasme* as a catalyst for more recent, cryptic speciation. Leveraging population genomics, we studied how the Pleistocene glaciation and ecological phenomena affected the evolutionary dynamics of mountainous plants. By examining restriction-site association DNA (RAD loci), we found four distinct lineages evolving separately as cryptic species. This research highlights the ice age's role in the cryptic speciation of regional plant diversity. Additional plant phylogenomic data and evolutionary timelines further confirm that separate evolution caused the remarkable macro-diversity in mountain plants.

RESULTS

Genomic consequences of *Stellera chamaejasme*-cryptic species morphs

High-throughput sequencing was performed on 251 individuals from four unique species morphs of *S. chamaejasme*, yielding an average of over 3.76 million raw reads (Figure 2B–E). After ensuring quality, approximately 3.47 million reads were utilized, leading to the identification of 23,215 RAD loci with 5,800 single nucleotide polymorphisms (SNPs) through *de novo* assembly (Table S1). Grouping the individuals into four cryptic species morphs for the Treemix analysis yielded 1,716 loci. Similarly, pruned datasets of 102 individuals for use in Bayesian phylogeny and phylogeography (BPP) resulted in 25,049 loci. The minimal genetic diversity at the population level was detected (Tables S2–S6), with the highest genetic diversity in the YY morph (Table S2). Notably, significant genetic differentiation was observed within cryptic species morphs, in the Deng8999 population ($\Phi_{ST} = 0.832$, $D_{XY} = 0.0058$, and $F_{ST}' = 0.824$) (Figure S1; Tables S4, S5). However, the population of the same cryptic species morph had little genetic differentiation (Figure S1).

The cluster analysis using fastSTRUCTURE identified 34 populations as belonging to four ancestral groups ($K = 4$) (Figures 3A, S2). At a different analytical level ($K = 2$), an admixed YW morph population was found (Figures 3A, S2B). Both discriminant analysis of principal components (DAPC)

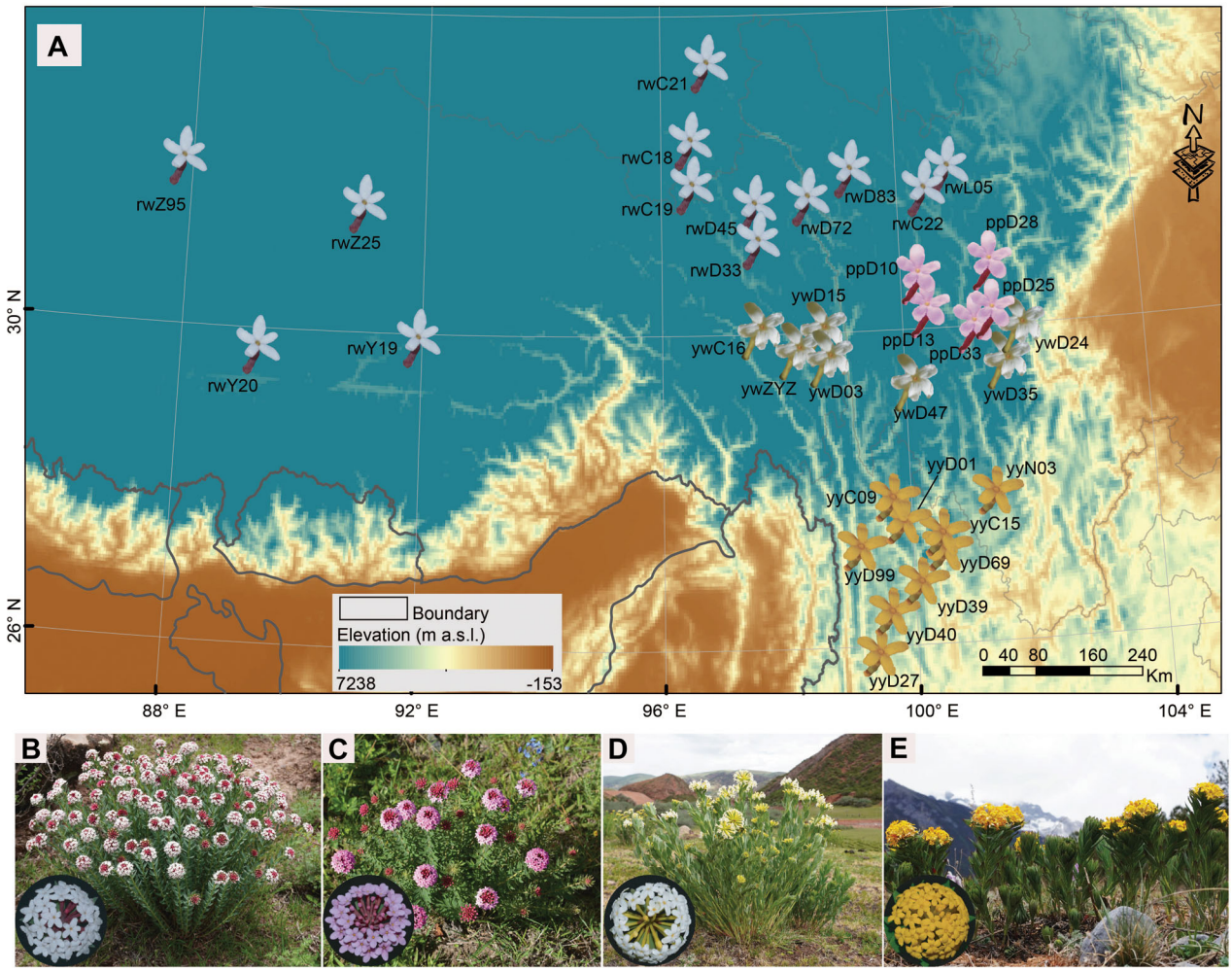

Figure 2. Geographic distribution of populations sampled to infer cryptic speciation in *Stellera chamaejasme*

(A) The 34 populations of *S. chamaejasme* were sampled across the Hengduan Mountains - Qinghai-Tibet Plateau (HM-QTP) complex (details in Table S2). The standard map of China with neighboring countries was used from http://bzdt.ch.mnr.gov.cn/index.html (map approval number: GS (2022)4314). The four species morphs are **(B)** red-white morph (RW), **(C)** pure pink morph (PP), **(D)** yellow-white morph (YW), and **(E)** pure yellow morph (YY); and coded the same throughout the Figures unless specified for other colors. (Note: geographic data in this study used an Albers projection based on the "GCS_krasovsky 1940" geographic coordinate system.)

(Figure 3B) and principal component analysis (PCA) (Figure S3) confirmed the genetic groups identified by fastSTRUCTURE, with the Deng9783 population standing out from the PP morph, possibly due to missing data and a limited number of loci. A deeper Bayesian fine RAD structure with the shared co-ancestry matrix analysis supported the existence of the four separate genetic clusters ($K = 4$) (Figure S4), showing notable genetic differentiation.

Coalescent tree inference and species delimitation

The phylogenomic analysis using IQ-TREE (Figures S5, S6) using the best substitution model (Table S7) and MrBayes (Figure S7) highlighted four major clades that correspond to the four species morphs. Although the support values for these clades differed (bootstrap support >86% and SH-aLRT >71), they were robust, with a clear division between the red (RW and PP morphs) and the yellow type (YW and YY morphs). The PP morph was more localized, while the RW morph had a wider spread. The HM endemic yellow type emerged as a distinct lineage nested within the YW morph populations. Notably, the Deng9783 population aligned more with the RW morph, contradicting its grouping with the PP morph in earlier fastSTRUCTURE results.

Using BPP for species delimitation, we primarily centered on a model that recognizes four cryptic species morphs; although there were alternate models with fewer species, their support was notably less (Table S8). The most supported two-species model grouped RWPP and YWYY morphs, with the highest probability of 0.42 under the prior $\theta \sim G(2, 0.4)$ $\tau \sim G(2, 0.002)$. For the four-species model, the posterior probability ranged relatively low from 0.26 to 0.30 across the range of considered priors, emphasizing weak support for four morphs being species. This further supports the recognition of four morphs as cryptic species, rather than being

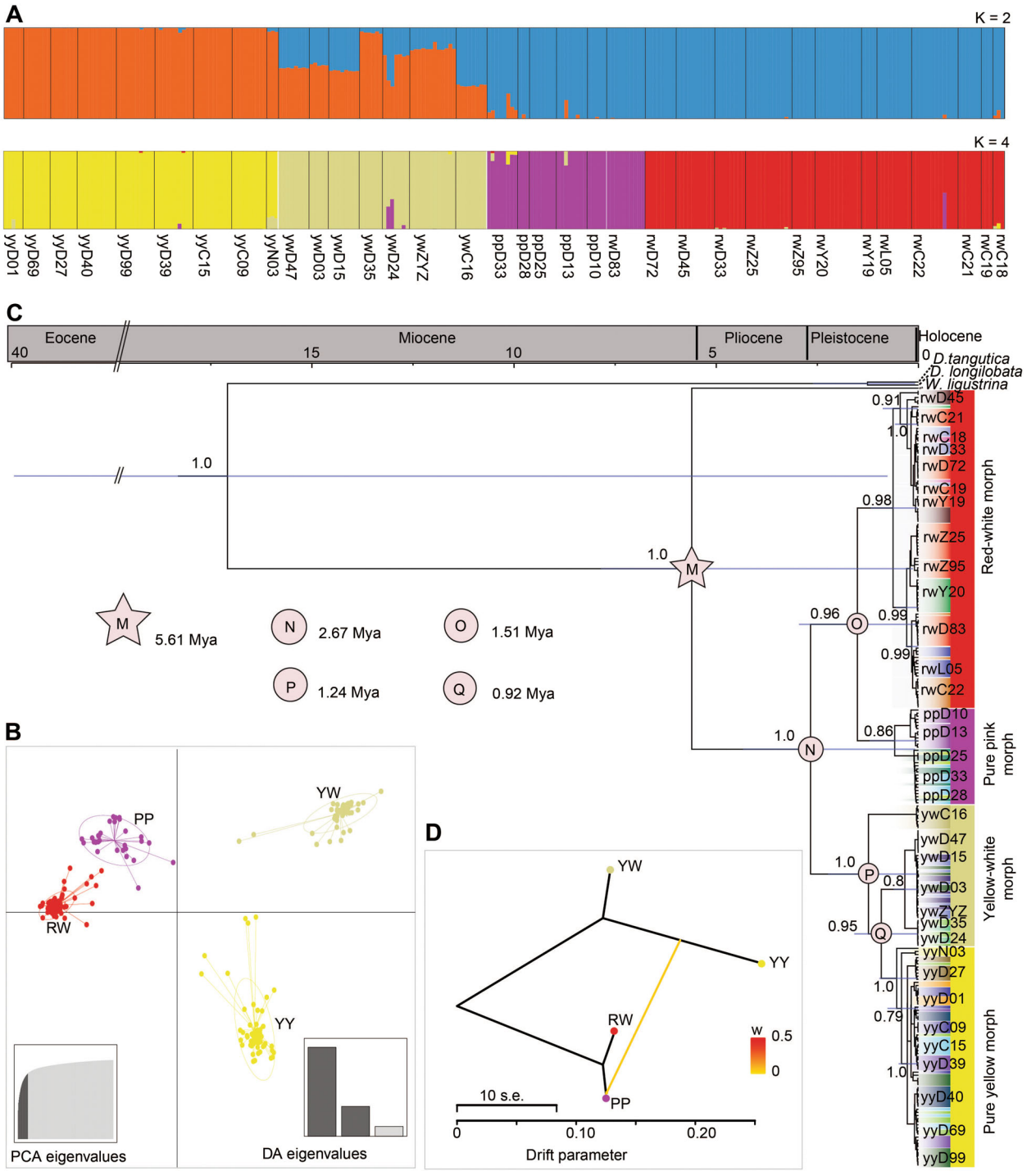

Figure 3. Tempo of species diversification in *Stellera chamaejasme*

(A) Hierarchically structured clusters were computed using fastSTRUCTURE under $K = 2$ and $K = 4$. Colors indicate the posterior probability of an assigned individual to a particular cluster. **(B)** Genetic clusters of four cryptic species morphs were analyzed using discriminant analysis of principal components (DAPC). **(C)** An estimated divergence time was inferred using a Bayesian multi-species coalescent method. The relevant estimated stem age (color star, M) and crown ages (color circles, N–Q) of the cryptic species morph of *S. chamaejasme* are represented in corresponding nodes. Blue bars represent the 95% highest posterior density intervals for node ages, and values near nodes indicate posterior probabilities of the major nodes. **(D)** Gene flow between the cryptic species morph was estimated using TREEMIX. A colored arrow line represents the direction of gene flow. The horizontal scale bar at the bottom (drift parameter) shows the entries' 10-fold average standard error, and the color scale shows the migration weight *w*. Each species morph was coded the same throughout the figures unless specified for other colors.

biological species. Further, BFD* (Bayes Factor Delimitation, *with genomic data) demonstrated increasing support for a model that divided individuals into four cryptic species morphs (Table 2). The BFD results showed increasing likelihood and $2lnBF > 10$ as the number of species increased, supporting a model where individuals are divided into four cryptic species morphs (consistent with clustering under $K = 4$ and tree estimation). However, a two-species model could also be plausible under certain conditions as compared to a four-species model. The convergence of the analysis was affirmed by examining likelihood traces, ensuring the mean effective sample size (ESS) per model ≥165 (Table S9).

The tempo of species diversification

The divergence of *S. chamaejasme* from the closely related taxon *Wikstroemia ligustrina* was estimated to have occurred in the Late Miocene (c. 5.61 Mya; 95% highest posterior density (HPD) intervals, 0.13–7.85 Mya). The formation of species morphs within *S. chamaejasme* began around the Late Pliocene (c. 2.67 Mya; 95% HPD: 0.008–4.34 Mya) (Figure 3C). Two major clades (red type and yellow type) were discerned, which further split into four sub-lineages representing the cryptic species morphs (posterior probability ≥ 0.95). Their divergence mainly took place in the Middle Pleistocene (c. 1.51–0.92 Mya). The RW and PP morphs separated c. 1.51 Mya (95% HPD: 0.04–2.95 Mya), while the YW morph, being polyphyletic, showed a divergence of one sub-lineage (Chen0016) at c. 1.24 Mya (95% HPD: 0.04–2.24). Another sub-lineage of YW was nested within the YY morph, indicating a more recent divergence c. 0.92 Mya (95% HPD: 0.02–1.59) (Figure 3C).

The chord diagram reflects clear genetic differentiation among these morphs, with the most significant difference seen between the red (RW/PP) and yellow (YW/YY) types (Figure S1). Limited migration events with lesser weight (Figure 3D) were observed between the PP and YY morphs, while other cryptic species morphs showed no discernible gene flow. There were evident isolation-by-distance (IBD) patterns, suggesting that geographic distance impacts the genetic structure of *S. chamaejasme*, supported by a Mantel test ($r = 0.48$, $P = 0.0001$***) (Figure S8A). While within each species morph, the IBD pattern was mostly insignificant (Figure S8B, D, E), except for the PP morph ($r = 0.89$, $P = 0.0167$*) (Figure S8C).

The mode of species diversification

Genealogical unsupervised machine learning clustering using randomForest (RF) and t-distributed stochastic neighbor embedding (t-SNE) analyses consistently clustered *S. chamaejasme* into four species morphs, supporting earlier results (Figures S9). Notably, these approaches clarified the discrepancy of the RW morph's Deng9783 population being grouped with the PP morph, a finding that fastSTRUCTURE hinted at but other approaches like classic multidimensional scaling (cMDS) (Figure S9E) and t-SNE plot (Figure S9F) further elucidated. Notably, MDS and isotonic MDS (isoMDS) exhibited high variability and clustering among the morphs, with few exceptions for cMDS. While each clustering technique and ordination approach demonstrated unique characteristics, the optimal clustering was a four-clusters ($K = 4$) division for *S. chamaejasme*, confirmed by K-means and PAM (partition around medoids) clustering (Figure S9A, B) indices.

Characterizing the phenotypes, we evaluated 29 morphological traits (16 continuous, 13 categorical, most of which were non-normal ($P < 0.05$), except PP morph) (Table S10) and uncorrelated (Figure S10). While continuous traits like a rhizome, stem lengths, and leaf length-width ratio displayed varied distributions across the species morphs, categorical traits showed differences, with exceptions like leaf apex, flower number, and bract number (Figure S11). Using a multivariate analysis of variance (MANOVA) test, assuming homogeneity of variance (Table S11), these traits effectively delimited the species morphs (Table S12) (F-stat = 17.60, $P < 2.2e^{-16}$). However, certain traits, such as rhizome length, petiole length, lobe length-width ratio, bract number, and flower number, did not significantly differentiate species (at significance level 0.05). Tukey's *post hoc* test highlighted categorical traits, like leaf shape, leaf base, lobe color, and mid-rib color for all paired species except RW and YW (Table S13), as more effective differentiators than continuous ones. Among the continuous traits, leaf length-width ratio and leaf width base-apex ratio significantly differentiated the highest number of paired species ($P < 0.05$) (Table S13).

Table 2. Species delimitation results from BFD* (Bayes factor delimitation, *with genomic data) in 251 individuals of *Stellera chamaejasme* and three closely related taxa (*Daphne longilobata* (Lecomte) Turrill, *Daphne tangutica* Maxim, *Wikstroemia ligustrina* Rehder; not shown) with 5,800 unlinked, bi-allelic single nucleotide polymorphisms

Scenarios	Species delimitation model	Marginal L estimate (MLE)	*Ln* (BF)	*2ln* (BF)	Rank
Null model	Current taxonomy: RWPPYWYY	−110383.59	–	–	–
Alternative 1	Splitting (red and yellow morph): 2-species: RWPP-YWYY	−68459.59	41924.00	83848.00	4
Alternative 2	Splitting (yellow morph): 3-species: RWPP-YW-YY	−32336.66	78046.93	156093.86	2
Alternative 3	Splitting (red morph): 3-species: RW-PP-YWYY	−36962.92	73420.67	146841.34	3
Alternative 4	#Splitting (red-white, pure red, yellow-white, and pure yellow morph): 4-species: RW-PP-YW-YY	−19020.89	91362.70	182725.40	1

Note: Bayes factors (*2ln*(BF)) were calculated as 2×(MLEalternatives - MLEnull); # the best-supported models; four cryptic species morphs are RW, red-white morph; PP, pure pink morph; YW, yellow-white morph; YY, pure yellow morph.

Trait-based visualizations (traitgrams) highlighted differentiation and overlap in the leaf width basal-apex ratio and leaf shape (Figures 4A, S12). PCA confirmed the distinctiveness of the four cryptic species of *S. chamaejasme*, with some overlaps across certain morphs (Figures 4B, S13A, B). Notably, the RW morph is distinct in traits like leaf width base-apex ratio, flowering season, leaf angle, and stem number, while the PP morph is differentiated mainly by leaf density. Traits excluding stem length, bract length, and leaf area are pivotal in distinguishing the YW and YY morphs (Figure 4B). The linear discriminant analysis (LDA), accounting for 99.87% of the total variation (Figure S13C), indicated categorical traits as the main differentiators over the mean values of continuous traits. However, due to the presence of major overlapping morphological traits, it fails to clearly delimit those morphs as species morphologically.

Ecologically, the range of the four cryptic species morphs was determined using the least correlated predictive variables (Tables S14–S16). The PCA demonstrated that 39.60% of the total variation is captured by PC1 accounting for 21.50% and PC2 accounting for 18.10% (Figure S14A). PCA biplots showed that the RW and YY morphs are differentiated by multiple variables, while the PP and YW morphs are influenced by specific variables (Figure S14A, C–F). For instance, habitat heterogeneity predominately defines the RW morph, while the YY morph is influenced more by ultraviolet radiation (Figure S14A, C–F). LDA reinforced this grouping, with LD1 capturing 61.41% of the variation (Figure S14B). Variables crucial for all morphs encompass bioclimatic factors, geo-climatic variables, habitat heterogeneity measures, and land cover characteristics. The predictive ensemble species distribution modeling (eSDM) (Table S17) highlighted potential distribution areas for these morphs in the HM-QTP region, emphasizing the major biodiversity hotspots of HM and northeast China (Figure 4C). While the PP and YW morphs coexist in the eastern HM (Figure 2A), the RW morph is more widespread across the Himalayas, the QTP, the northwestern range of the HM and northeast China (Figure 4C). From the last glacial maximum (LGM, ~22,000 years BP) to the current climatic scenario (c. 1990–2000), all morphs have expanded their suitable habitats (Figure S15). Notably, the niche similarity test having relatively low to moderate overlap (D, $I < 0.7$), emphasizes that while species may share a habitat, they do not entirely overlap in their ecological preferences or requirements, potentially reducing interspecific competition (Figures S16). This further exemplifies that the RW morph is potentially suited to broader regions like the Himalayas, the QTP, and northeast China, whereas the other morphs are primarily confined to the HM with shared habitat.

DISCUSSION

Cryptic speciation in understanding the mountains of Southwest China's plant diversity

The plant diversity in the mountains of Southwest China is intricately tied to cryptic speciation (Liu et al., 2013, 2019). Despite evidence of species formation, the clarity in taxonomic identification is uncertain, enhancing their crypticity. This reveals insights into the evolving species shaping these biodiversity hotspots. In *S. chamaejasme*, deep genetic divergence underlies morphological similarities, indicating advanced stages of speciation. Our research highlights the significant role of allopatric speciation, evidenced by four distinct metapopulation lineages in *S. chamaejasme*. However, there is potential for sympatric coexistence because the morphs are not competing intensely for the same resources. The driving forces behind the reproductive isolation of different lineages are genomic evolution and inherent genomic incompatibilities (Zhang et al., 2011b; Wen et al., 2014; Struck et al., 2018; Dufresnes et al., 2021). While these lineages are geographically separated and recently diverged, suggesting they could be cryptic species, their classification under the biological species concept is challenging (Fišer et al., 2018) and further accentuate the need to recognize the emerging species (de Queiroz, 2007). This concept stresses reproductive isolation and distinct morphological traits as key to defining species. Nonetheless, *S. chamaejasme*'s indistinct morphological traits and ongoing speciation process hint at the presence of four cryptic species, aligning with de Queiroz's unified species concept (de Queiroz, 2007).

In the HM, many plants once thought to be single species, are now being recognized as cryptic species, in the midst of evolving into separate entities (Li et al., 2021; Ma et al., 2021; Zhao et al., 2021; Liu et al., 2022; Sun et al., 2022) (Table 1). This is particularly evident in the case of *S. chamaejasme*. This species exhibits significant genetic differentiation and clear clades correlating with morphological variations. Speciation here is often driven by historical geographic or environmental factors, leading to allopatric divergence. Yet, the unclear morphological differences and presence of relatively low supports of species delimitation among the four color morphs (RW, PP, YW, and YY) of *S. chamaejasme*, along with recent divergence (Hu et al., 2022) and less mobile pollinators (Zhang et al., 2011b; Van der Niet et al., 2014; Zhang et al., 2021a), suggest they do not fully meet traditional criteria for distinct biological species. Pollinator interactions in *S. chamaejasme* may not rely on floral color, suggesting that common Lepidopterans (butterfly and moths) have a limited role in cryptic speciation (Zhang et al., 2011b). Conversely, a distinct brood-pollination mutualism with *Frankliniella intonsa* (Trybom) highlights how specialized pollinator relationships contribute to reproductive isolation and genetic differentiation (Zhang et al., 2021a). Furthermore, self-incompatibility and flower specialization stress the need for specific habitats for effective pollination and reproduction, fostering population isolation and evolutionary divergence (Zhang et al., 2011b).

Yet, this revelation comes with a conservation caution: species that are evolving yet unrecognized may be vulnerable to threats (Alizon et al., 2008), as exemplified by the PP morph with its unique habitat needs. Incorporating the insights gained from our study on cryptic speciation in Southwest China's mountainous ecosystems offers a pivotal

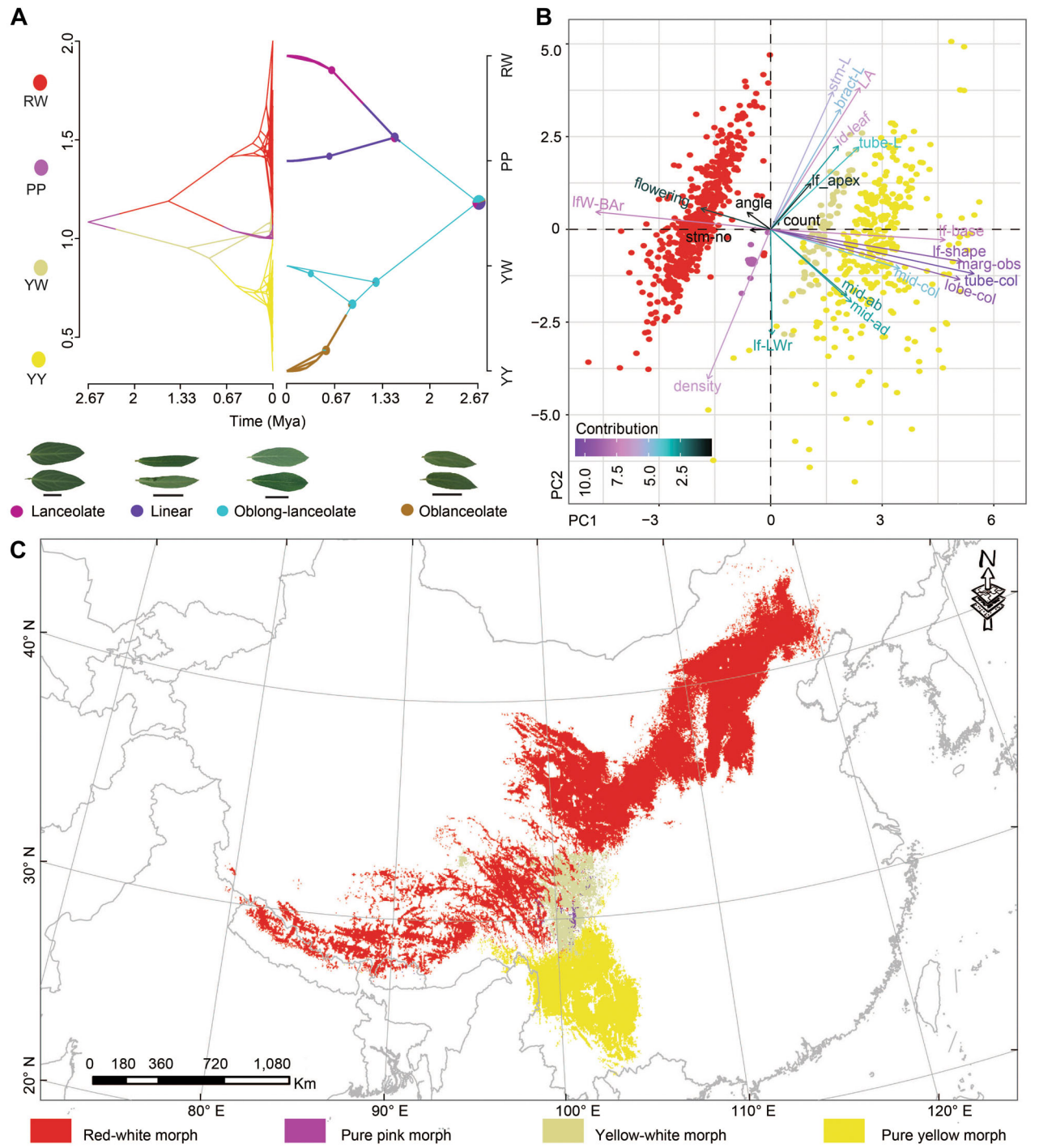

Figure 4. Mode of species diversification in *Stellera chamaejasme*

(A) Traitgram depicting the temporal differentiation was mapped over dated Markov chain Monte Carlo tree (time from the root: x-axis) using leaf character (presented as photo plates) categorized as a continuous trait-ratio of leaf width at basal/apex region (lfW_B/Ar) (trait value: y-axes; left side) and categorical trait-leaf shape (species: y-axes; right side). **(B)** The relative contributions of morphological traits to the principal components (PC1, 27.6%; PC2, 12.0%) according to the cryptic species morph was inferred through principal component analysis (PCA) biplots. **(C)** Ecological niche dynamics are predicted by ensemble species distribution modeling (eSDM) under current scenarios of environmental variables, as a measure of cryptic species morphs differentiation in *S. chamaejasme*. The standard map of China with neighboring countries was used from http://bzdt.ch.mnr.gov.cn/index.html (map approval number: GS (2022)4314). (Note: geographic data in this study used an Albers projection based on the "GCS_krasovsky 1940" geographic coordinate system.)

perspective on biodiversity conservation strategies in similarly affected mountainous regions globally. Understanding the specialized pollinator interactions and habitat specialization is vital for formulating conservation measures that can anticipate and mitigate the impacts of rapid climate change. Therefore, identifying these cryptic species is critical not only for scientific advancement but also for devising a blueprint for effective conservation strategies in biodiversity hotspots considering the tempo and mode of cryptic speciation (Bickford et al., 2007; Chen et al., 2019).

Recent Pleistocene glaciation: A crucible for cryptic speciation in *S. chamaejasme*

The mountains of Southwest China complex is renowned worldwide for its rich biodiversity, offering a unique canvas to study the distribution of biological communities (Sun et al., 2017). While past research linked the region's species formation to older geological events at 8–10 Mya (Spicer et al., 2003; Deng and Ding, 2015; Ding et al., 2020), or ancient monsoonal activities around 5.30 Mya (Liu et al., 2015; Farnsworth et al., 2019), our study attributes recent Pleistocene glaciation as a significant influencer. Specifically, *S. chamaejasme*'s lineage originated in the Late Miocene (around 5.61 Mya) but diversified during the Pleistocene (around 2.67 Mya), a period after the Hengduan Mountains reached their current elevation, highlighting how the region's established high elevation and environmental heterogeneity facilitated the species' cryptic speciation. Our data indicate that these changes during the Pleistocene period bolstered genetic variations, leading to the emergence of newer cryptic species at a young age perfectly tailored to their environments.

Specifically, the YY type emerged around 0.92 Mya, affected by the climate of that epoch. As the LGM progressed, the YW morph evolved, while the YY morph migrated southward to warmer areas. The RW morph persisted due to HM's glacial events, and the PP morph took refuge in valleys. With warming during the interglacial phase, RW moved north to colder regions, eventually diversifying its lineages. This adaptation during the ice age led to the current distribution of the four cryptic species morphs (shown in Figure 1B). Notably, ice-free pockets of land served as refugia for many alpine plants during glaciation (Pointing et al., 2014) in the biodiversity hotspot—the mountains of Southwest China (Mittermeier et al., 2011), highlighting the Pleistocene's role in shaping the region's evolutionary history. The emergence, adaptation, and migration of the four cryptic species morphs in *S. chamaejasme* during this period are a testament to the resilience and adaptability of plants in this biodiversity-rich region.

Pleistocene-driven diversification: The north-south and elevational migration model

Many diversification studies have overlooked the Pleistocene's role in speciation, primarily focusing on geological events and monsoons (Levsen et al., 2012). The Pleistocene, characterized by drastic climate changes, had profound implications on mountain plant diversity. During the glacial period, decreased precipitation (Ou et al., 2014; Farnsworth et al., 2019) and ice-free temperature conditions (Zhou et al., 2006; Liu et al., 2015) prompted plant diversification in the HM region. Starting around 2.67 Mya, the Pleistocene glaciation and climate fluctuations triggered species differentiation. The transition from the PP to RW morph was driven by northward and high-altitude shifts due to the warming events after the Xixiabangma Glaciation about 1.5 Mya (Zheng et al., 2002). In contrast, the YW to YY shift occurred due to southward and lower elevational migrations during the Naynayxungla Glaciation's cooling events (Shi and Ren, 1990; Zhou and Li, 1998). Despite evidence of limited glacial extensions in the HM between 0.46 and 0.71 Mya (Xu et al., 2010; Wang et al., 2017), the overall influence of the Pleistocene on current mountain plant diversity remains uncertain. This period likely fostered species diversification, especially through allopatric speciation in presence of geographically isolated mountains (Liu et al., 2013, 2019, 2022; Smyčka et al., 2022). These migrations, influenced by geographical habitats, led to species variations like the high-altitude RW morph versus the valley-dwelling PP. Barriers, such as tree lines, separated habitats like the high-altitude YW and the lower-altitude YY morph, ensuring genetic distinctiveness by reducing gene flow.

Beyond the glaciation events for diversification, the migratory patterns, both north-south and elevational, of the cryptic species in *S. chamaejasme* provide a richer understanding of how climatic shifts shaped the evolution of plant species in the HM region (Figure 1B). The north-south orientation of the HM valleys, as opposed to the Himalayas, QTP's east-west alignment, indicates lower extinction and consistent southward migration during Pleistocene glaciation. After this era, drainage pathways enabled plant migration from higher to lower terrains (Wang et al., 2015; Rana et al., 2020), causing shifts in ideal habitats and enhancing genetic diversity, evidenced by the emergence of the YY morph. Glacial retreats resulted in reproductive adaptations (Liu et al., 2019), producing four distinct cryptic species forms under ice age conditions (Figure 1B). Some species morphs, like YW and RW, moved lower during colder times and higher during warmth, forming adapted populations like YY and PP morphs. While Pleistocene glaciations played a role, barriers like the MSD (Ward, 1921; Luo et al., 2017), the 29°N latitude line (Zhang et al., 2009), and the Tsangpo-Brahmaputra Grand Canyon (TBGC) (Rana et al., 2023) also influenced species diversification in *S. chamaejasme*. The north-south and elevational migration models during the glaciation periods offer novel perspectives on Pleistocene-driven diversification and the combined impacts of glaciation and biological factors (e.g., pollinators) on speciation in the HM.

The biodiversity of the mountains of Southwest China is deeply intertwined with the phenomenon of cryptic speciation. Although numerous plants in this region might seem similar in their physical appearance, their genetic makeup and overlapping morphological traits indicate they are on the

verge of becoming a distinct species. Our research provides an emphasis on the significance of the recent Pleistocene glaciation and interactions with pollinators in shaping cryptic speciation. Contrary to older hypotheses of ancient assemblage of the HM flora, we suggest a more recent emergence of floral diversity largely driven by allopatric speciation during Pleistocene environmental changes. The geological transformations resulting after the uplift of the HM, combined with Pleistocene climate changes, have been instrumental in driving this genetic divergence and the emergence of cryptic species. Key migration patterns, both north-south and elevational, further highlight the nuanced process of species formation in the area. Ultimately, understanding this complex interplay of factors is not just pivotal for advancing scientific comprehension but also for crafting conservation strategies to protect the burgeoning biodiversity of the region.

MATERIALS AND METHODS

Sampling, RAD sequencing, and data processing

Sampling of plant material was strategically designed to support the study of cryptic speciation, a process where genetically distinct species exhibit similar morphologies. To identify cryptic species morphs, we focused on discerning significant genetic divergence, subtle morphological differences, and ecological variances, notwithstanding their seemingly indistinguishable appearances. Total genomic DNA was extracted from silica gel-dried leaves of 34 *S. chamaejasme* populations and three outgroups using a Plant Genomic DNA Kit (Tiangen, China). For adaptability and high resolution of genetic data, the extracted DNA was used to construct RAD-seq libraries, which were then sequenced on two lanes of the Illumina HiSeq. 2000 platform (Illumina, San Diego, CA, USA). The clean sequencing reads have been deposited in the National Center for Biotechnology Information (NCBI) Sequence Read Archive in the Bioproject (PRJNA1002599). After filtering and processing the clean reads, *de novo* assemblies were generated using *Stacks* v.2.55 (Catchen et al., 2013).

Genomic screening

Genetic diversity (π, H_e, H_o, F_{IS}) and population genetic differentiation (mean Φ_{ST}, D_{XY}, F_{ST}') indices were calculated using the *populations* pipeline in *Stacks* v.2.55. The most likely historical genetic clusters were inferred using Bayesian *fastSTRUCTURE* v.2.3.4 (Raj et al., 2014), and more contemporary components were identified through DAPC and PCA using the *adegenet* v2.1.3 (Jombart, 2008). Additionally, shared ancestry was estimated using *fineRADstructure* v.0.3.2 (Malinsky et al., 2018).

By utilizing likelihood and Bayesian approaches with *IQ-TREE* v.2.1.4_beta (Nguyen et al., 2015) and *MrBayes* v.3.2.7 (Ronquist et al., 2012), respectively, a concatenated supermatrix was employed to determine the phylogenomic relationships among 251 individuals of *S. chamaejasme*. *TreeMix* v.1.13 (Pickrell and Pritchard, 2012) was employed to infer historical relationships and gene flow among putative cryptic species morphs. Additionally, the multi-species coalescent model in *Beast2* v.2.6.3 (Bouckaert et al., 2014) was used to estimate a species tree and divergence times for the cryptic species using temporal calibration with two fossil calibrations for the root age of *S. chamaejasme* (Zhang et al., 2010). The significance of genetic divergence between the cryptic species of *S. chamaejasme* was assessed using linear models with geographic distance for IBD, implemented with the Mantel function in *vegan* v2.5-7 (Oksanen, 2021).

From the total pool of 251 individuals sampled, a subset of 102 individuals was pruned (pruned to include three individuals from each of 34 populations) for *population* call in *Stacks*, which was then used in the species delimitation BPP analysis. We then employed the reversible-jump Bayesian Markov chain Monte Carlo (rjMCMC) method (Yang and Rannala, 2010; Yang, 2015) using the multi-species coalescent (MSC) model in *BPP* v.4.4.0 (Rannala and Yang, 2013) to determine cryptic species delimitation and validate taxonomic classifications. Furthermore, the Bayes factor delimitation (BFD*) method (Grummer et al., 2014) was utilized to objectively compare and validate the alternative species delimitation models against the current taxonomy of *S. chamaejasme* in *Beast2* v2.6.3. Additionally, genomic clustering was performed using UML approaches, specifically RF and t-SNE (Derkarabetian et al., 2019).

Morphological characterization

We visualized 29 morphological traits (16 continuous and 13 categorical) from 950 herbarium specimens using ridgeplot in *ggridges* v.0.5.2 (Wilke, 2020), and we performed a multivariate statistical test to assess variation among the putative cryptic species in R v.3.6.3 (R Core Team, 2021), and visualized significant traits with traitgram in *phytools* v.0.7-70 (Revell, 2012) using the dated MCMC trees. Morphological traits were further analyzed using PCA and LDA to assess the relative contribution of traits to the hypothesized four cryptic species.

Ecological niche dynamics

The collated species occurrence data from herbaria, field records, and online databases were used for eSDM using *Biomod2* v3.4.12 (Braconnot et al., 2007). Models were built using spatially rarefied 307 out of 363 occurrence points and 10,000 random pseudo absence points. The potential distribution of four cryptic species was modeled for the current climatic scenario (c. 1990–2000) and projected to paleoclimatic (LGM c. 22 kya) scenario (Thuiller et al., 2020) using least correlated predictive variables. The predictive variables were further analyzed using PCA and LDA to evaluate the relative contributions and discriminate the four cryptic species. An ensemble of the 10 algorithms was generated using the model with model accuracy ≥ 0.80, and the consensus model was converted to a binary model with a 50% probability threshold of suitable habitat that suits the present distribution of the focal species. Niche equivalency testing was performed using the ecospat function in *ENMTools* v.1.0.3

(Warren and Dinnage, 2021; Warren et al., 2021) along the projected niche of *S. chamaejasme*.

See supplementary Methods for more details.

Data availability statement

Clean sequence reads obtained by RAD-seq were deposited in the NCBI Sequence Read Archive in the Bioproject PRJNA1002599 (https://www.ncbi.nlm.nih.gov/bioproject/PRJNA1002599). All other study data used in the manuscript are available at https://github.com/santoshkumarrana/Pleistocene-glaciation-for-cryptic-speciation-in-Stellera.

ACKNOWLEDGEMENTS

We thank Zhen-Yu Lv for field assistance, and Ms. Song Minshu for laboratory assistance. This study was funded by the Second Tibetan Plateau Scientific Expedition and Research (STEP) program (2019QZKK0502), the Key Projects of the Joint Fund of the National Natural Science Foundation of China (U23A20149), the Research Fund for International Young Scientists of the National Natural Science Foundation of China (32150410356), National Natural Science Foundation of China (32322006), the Young Academic and Technical Leader Raising Foundation of Yunnan Province (2019HB039), and the International Association for Plant Taxonomy (IAPT) Research grant (421064806). The first author is supported by the "CAS President's International Fellowship Initiative" (PIFI) postdoctoral fellowship (2021PB0034).

CONFLICTS OF INTEREST

The authors declare no conflicts of interest.

AUTHOR CONTRIBUTIONS

H.S., C.D., and T.D. designed research; S.K.R., H.K.R., and J.C. performed research sampling; S.K.R., H.K.R., and T.K. analyzed data; and S.K.R. wrote the paper with the support of H.S., C.D., T.D., J.B.L., and H.W. All authors read and approved the content of this manuscript.

Edited by: Bojian Zhong, Nanjing Normal University, China

Received Jan. 23, 2024; **Accepted** Mar. 26, 2024

REFERENCES

Alizon, S., Kucera, M., and Jansen, V.A.A. (2008). Competition between cryptic species explains variation in rates of lineage evolution. Proc. Natl. Acad. Sci. U.S.A. **105:** 12382–12386.

Bickford, D., Lohman, D.J., Sodhi, N.S., Ng, P.K., Meier, R., Winker, K., Ingram, K.K., and Das, I. (2007). Cryptic species as a window on diversity and conservation. Trends. Ecol. Evol. **22:** 148–155.

Bouckaert, R., Heled, J., Kühnert, D., Vaughan, T., Wu, C.H., Xie, D., Suchard, M.A., Rambaut, A., and Drummond, A.J. (2014). BEAST2: A software platform for Bayesian evolutionary analysis. PLoS Comput. Biol. **10:** e1003537.

Braconnot, P., Otto-Bliesner, B., Harrison, S., Joussaume, S., Peterchmitt, J.Y., Abe-Ouchi, A., Crucifix, M., Driesschaert, E., Fichefet, T., Hewitt, C.D., et al. (2007). Results of PMIP2 coupled simulations of the Mid-Holocene and Last Glacial Maximum—Part 1: Experiments and large-scale features. Clim. Past **3:** 261–277.

Catchen, J., Hohenlohe, P.A., Bassham, S., Amores, A., and Cresko, W.A. (2013). Stacks: An analysis tool set for population genomics. Mol. Ecol. **22:** 3124–3140.

Chen, J.H., Huang, Y., Brachi, B., Yun, Q.Z., Zhang, W., Lu, W., Li, H.N., Li, W.Q., Sun, X.D., Wang, G.Y., et al. (2019). Genome-wide analysis of Cushion willow provides insights into alpine plant divergence in a biodiversity hotspot. Nat. Commun. **10:** 5230.

Chen, Y.S., Deng, T., Zhou, Z., and Sun, H. (2018). Is the East Asian flora ancient or not? Nat. Sci. Rev. **5:** 920–932.

de Queiroz, K. (2007). Species concepts and species delimitation. Syst. Biol. **56:** 879–886.

Deng, T., and Ding, L. (2015). Paleoaltimetry reconstructions of the Tibetan Plateau: Progress and contradictions. Nat. Sci. Rev. **2:** 417–437.

Derkarabetian, S., Castillo, S., Koo, P.K., Ovchinnikov, S., and Hedin, M.A. (2019). A demonstration of unsupervised machine learning in species delimitation. Mol. Phylogenet. Evol. **139:** 106562.

Ding, W.N., Ree, R.H., Spicer, R.A., and Xing, Y.W. (2020). Ancient orogenic and monsoon-driven assembly of the world's richest temperate alpine flora. Science **369:** 578–581.

Dufresnes, C., Brelsford, A., Jeffries, D.L., Mazepa, G., Suchan, T., Canestrelli, D., Nicieza, A., Fumagalli, L., Dubey, S., Martínez-Solano, I., et al. (2021). Mass of genes rather than master genes underlie the genomic architecture of amphibian speciation. Proc. Natl. Acad. Sci. U.S.A. **118:** e2103963118.

Eaton, D.A.R., Fenster, C.B., Hereford, J., Huang, S., and Ree, R.H. (2012). Floral diversity and community structure in *Pedicularis* (Orobanchaceae). Ecology **93:** S182–S194.

Farnsworth, A., Lunt, D.J., Robinson, S.A., Valdes, P.J., Roberts, W.H., Clift, P.D., Markwick, P., Su, T., Wrobel, N., Bragg, F., et al. (2019). Past East Asian monsoon evolution controlled by paleogeography, not CO_2. Sci. Adv. **5:** eaax1697.

Fišer, C., Robinson, C.T., and Malard, F. (2018). Cryptic species as a window into the paradigm shift of the species concept. Mol. Ecol. **27:** 613–635.

Grummer, J.A., Bryson, R.W., and Reeder, T.W. (2014). Species delimitation using Bayes factors: Simulations and application to the *Sceloporus scalaris* species group (Squamata: Phrynosomatidae). Syst. Biol. **63:** 119–133.

He, K., and Jiang, X.L. (2014). Sky islands of southwest China. I: An overview of phylogeographic patterns. Chin. Sci. Bull. **59:** 585–597.

Hu, H., Yang, Y., Li, A., Zheng, Z., Zhang, J., and Liu, J. (2022). Genomic divergence of *Stellera chamaejasme* through local selection across the Qinghai-Tibet Plateau and northern China. Mol. Ecol. **31:** 4782–4796.

Huang, S.C. (1985). Taxa nova Thymelaeacearum sinicarum. Acta Bot. Yunnan **7:** 277–291.

Jin, Y., and Qian, H. (2019). V.PhyloMaker: An R package that can generate very large phylogenies for vascular plants. Ecography **42:** 1353–1359.

Jombart, T. (2008). adegenet: A R package for the multivariate analysis of genetic marker. Bioinformatics **24:** 1403–1405.

Léveillé, H. (1912). Decades plantarum novarum. Repert. Spec. Nov. Regni Veg. **10:** 581.

Levsen, N.D., Tiffin, P., and Olson, M.S. (2012). Pleistocene speciation in the genus *Populus* (Salicaceae). Syst. Biol. **61:** 401–412.

Li, L., Zhang, J., Lu, Z., Zhao, J.L., and Li, Q.J. (2021). Genomic data reveal two distinct species from the widespread alpine ginger *Roscoea tibetica*. J. Syst. Evol. **59:** 1232–1243.

Linnaeus, C. (1753). *Species plantarum*. Impensis Laurentii Salvii.

Liu, J., Möller, M., Provan, J., Gao, L.M., Poudel, R.C., and Li, D.Z. (2013). Geological and ecological factors drive cryptic speciation of yews in a biodiversity hotspot. New Phytol. **199:** 1093–1108.

Liu, R., Wang, H., Yang, J.B., Corlett, R.T., Randle, C.P., Li, D.Z., and Yu, W.B. (2022). Cryptic species diversification of the *Pedicularis siphonantha* Complex (Orobanchaceae) in the Mountains of Southwest China since the Pliocene. Front. Plant Sci. **13:** 811206.

Liu, X., Guo, Q., Guo, Z., Yin, Z.Y., Dong, B., and Smith, R. (2015). Where were the monsoon regions and arid zones in Asia prior to the Tibetan Plateau uplift? Nat. Sci. Rev. **2:** 403–416.

Liu, Y., Jin, W., Wei, X., and Wang, X.Q. (2019). Cryptic speciation in the Chinese white pine (*Pinus armandii*): Implications for the high species diversity of conifers in the Hengduan Mountains, a global biodiversity hotspot. Mol. Phylogenet. Evol. **138:** 114–125.

Luo, D., Xu, B., Li, Z.M., and Sun, H. (2017). The 'Ward Line–Mekong–Salween divide' is an important floristic boundary between the eastern Himalaya and Hengduan Mountains: Evidence from the phylogeographical structures of subnival herbs *Marmoritis complanatum* (Lamiaceae). Bot. J. Linn. Soc. **185:** 482–496.

Ma, Y.P., Wariss, H.M., Liao, R.L., Zhang, R.G., Yun, Q.Z., Olmstead, R. G., Chau, J.H., Milne, R.I., Van de Peer, Y., and Sun, W.B. (2021). Genome-wide analysis of butterfly bush (*Buddleja alternifolia*) in three uplands provides Insights into biogeography and speciation. New Phytol. **232:** 1463–1476.

Malinsky, M., Trucchi, E., Lawson, D.J., and Falush, D. (2018). RADpainter and fineRADstructure: Population inference from RADseq data. Mol. Biol. Evol. **35:** 1284–1290.

Mittermeier, R.A., Turner, W.R., Larsen, F.W., Brooks, T.M., and Gascon, C. (2011). Global biodiversity conservation: The critical role of hotspots. In *Biodiversity Hotspots*, F. Zachos, J. Habel, eds, (Berlin, Heidelberg: Springer), pp. 3–22.

Myers, N., Mittermeier, R.A., Mittermeier, C.G., da Fonseca, G.A.B., and Kent, J. (2000). Biodiversity hotspots for conservation priorities. Nature **403:** 853–858.

Nguyen, L.T., Schmidt, H.A., von Haeseler, A., and Minh, B.Q. (2015). IQ-TREE: A fast and effective stochastic algorithm for estimating maximum-likelihood phylogenies. Mol. Biol. Evol. **33:** 268–274.

Niu, Y., Stevens, M., and Sun, H. (2021). Commercial harvesting has driven the evolution of camouflage in an Alpine plant. Curr. Biol. **31:** 446–449.

Oksanen, J. (2021). Vegan: Community Ecology Package. R package Version 2.5-7. https://CRAN.R-project.org/package=vegan

Ou, X.J., Lai, Z.P., Zhou, S.Z., and Zeng, L.H. (2014). Timing of glacier fluctuations and trigger mechanism in eastern Qinghai–Tibetan Plateau during the late Quaternary. Quat. Res. **81:** 464–475.

Paudel, B.R., Shrestha, M., Burd, M., Adhikari, S., Sun, Y.S., and Li, Q.J. (2016). Coevolutionary elaboration of pollination-related traits in an alpine ginger (*Roscoea purpurea*) and a tabanid fly in the Nepalese Himalayas. New Phytol. **211:** 1402–1411.

Pickrell, J.K., and Pritchard, J.K. (2012). Inference of population splits and mixtures from genome-wide allele frequency data. PLoS Genet. **8:** e1002967.

Pointing, S.B., Bollard-Breen, B., and Gillman, L.N. (2014). Diverse cryptic refuges for life during glaciation. Proc. Natl. Acad. Sci. U.S.A. **111:** 5452–5453.

R Core Team (2021). *R: A language and environment for statistical computing. R Foundation for Statistical Computing*. https://www.R-project.org/

Rahbek, C., Borregaard, M.K., Antonelli, A., Colwell, R.K., Holt, B.G., Nogues-Bravo, D., Rasmussen, C.M., Richardson, K., Rosing, M.T., Whittaker, R.J., et al. (2019). Building mountain biodiversity: Geological and evolutionary processes. Science **365:** 1114–1119.

Raj, A., Stephens, M., and Pritchard, J.K. (2014). fastSTRUCTURE: Variational inference of population structure in large SNP data sets. Genetics **197:** 573–589.

Rana, H.K., Luo, D., Rana, S.K., and Sun, H. (2020). Geological and climatic factors affect population genetic connectivity in *Mirabilis himalaica*(Nyctaginaceae): Insight from phylogeography and dispersal corridors in the Himalaya-Hengduan biodiversity hotspot. Front. Plant Sci. **10:** 1721.

Rana, H.K., Rana, S.K., Luo, D., and Sun, H. (2023). Existence of biogeographic barriers for the long-term Neogene-Quaternary divergence and differentiation of *Koenigia forrestii* in the Himalaya-Hengduan Mountains. Bot. J. Linn. Soc. **201:** 230–253.

Rannala, B., and Yang, Z. (2013). Improved reversible jump algorithms for Bayesian species delimitation. Genetics **194:** 245–253.

Revell, L.J. (2012). phytools: An R package for phylogenetic comparative biology (and other things). Meth. Ecol. Evol. **3:** 217–223.

Ronquist, F., Teslenko, M., Van Der Mark, P., Ayres, D.L., Darling, A., Höhna, S., Larget, B., Liu, L., Suchard, M.A., and Huelsenbeck, J.P. (2012). MrBayes 3.2: Efficient Bayesian phylogenetic inference and model choice across a large model space. Syst. Biol. **61:** 539–542.

Shi, Y.F., and Ren, J.W. (1990). Glacier recession and lake shrinkage indicating a climatic warming and drying trend in central Asia. Ann. Glaciol. **14:** 261–265.

Smyčka, J., Roquet, C., Boleda, M., Alberti, A., Boyer, F., Douzet, R., Perrier, C., Rome, M., Valay, J.G., Denoeud, F., et al. (2022). Tempo and drivers of plant diversification in the European mountain system. Nat. Commun. **13:** 2750.

Spicer, R.A., Harris, N.B., Widdowson, M., Herman, A.B., Guo, S., Valdes, P.J., Wolfe, J.A., and Kelley, S.P. (2003). Constant elevation of southern Tibet over the past 15 million years. Nature **421:** 622–624.

Spicer, R.A., Su, T., Valdes, P.J., Farnsworth, A., Wu, F.X., Shi, G., Spicer, T.E., and Zhou, Z. (2020). Why 'the uplift of the Tibetan Plateau' is a myth? Nat. Sci. Rev. **8:** nwaa091.

Struck, T.H., Feder, J.L., Bendiksby, M., Birkeland, S., Cerca, J., Gusarov, V.I., Kistenich, S., Larsson, K.H., Liow, L.H., Nowak, M.D., et al. (2018). Finding evolutionary process hidden in cryptic species. Trends. Ecol. Evol. **33:** 153–163.

Sun, H., Li, Z., Landis, J.B., Qian, L., Zhang, T., and Deng, T. (2022). Effects of drainage reorganization on phytogeographic pattern in Sino-Himalaya. Alp. Bot. **132:** 141–151.

Sun, H., Zhang, J., Deng, T., and Boufford, D.E. (2017). Origin and evolution of plant diversity in the Hengduan Mountains, China. Plant Divers. **39:** 161–166.

Thuiller, W., Georges, D., Engler, R., and Breiner, F. (2020). Biomod2: Ensemble platform for species distribution modeling. R package version 3.4.12. https://cran.r-project.org/web/packages/biomod2/index.html

Tu, T., Volis, S., Dillon, M.O., Sun, H., and Wen, J. (2010). Dispersals of Hyoscyameae and Mandragoreae (Solanaceae) from the New World to Eurasia in the early Miocene and their biogeographic diversification within Eurasia. Mol. Phylogenet. Evol. **57:** 1226–1237.

Van der Niet, T., Peakall, R., and Johnson, S.D. (2014). Pollinator-driven ecological speciation in plants: new evidence and future perspectives. Ann. Bot. **113:** 199–211.

Wang, X.I.N., Chai, K., Liu, S., Wei, J., Jiang, Z., and Liu, Q. (2017). Changes of glaciers and glacial lakes implying corridor-barrier effects and climate change in the Hengduan Shan, southeastern Tibetan Plateau. J. Glaciol. **63:** 535–542.

Wang, Y., and Gilbert, M.G. (2007). *Stellera* L. In *Flora of China*, Z. Wu, P. H. Raven, D. Hong, eds, Volume **13** (St. Louis: Science Press, Beijing & Missouri Botanical Garden Press), p. 250.

Wang, Z.W., Chen, S.T., Nie, Z.L., Zhang, J.W., Zhou, Z., Deng, T., and Sun, H. (2015). Climatic factors drive population divergence and demography: insights based on the phylogeography of a riparian plant species endemic to the Hengduan Mountains and adjacent regions. PLoS One **10:** e0145014.

Ward, F.K. (1921). The Mekong-Salween divide as a geographical barrier. Geogr. J. **58:** 49–56.

Warren, D.L., and Dinnage, R. (2021). ENMTools: Analysis of niche evolution using niche and distribution models. R package version 1.0.3. https://cran.r-project.org/web/packages/ENMTools/index.html

Warren, D.L., Matzke, N.J., Cardillo, M., Baumgartner, J.B., Beaumont, L.J., Turelli, M., Glor, R.E., Huron, N.A., Simões, M., Iglesias, T.L., et al. (2021). ENMTools 1.0: An R package for comparative ecological biogeography. Ecography **44:** 504–511.

Wen, J., Zhang, J.Q., Nie, Z.L., Zhong, Y., and Sun, H. (2014). Evolutionary diversifications of plants on the Qinghai Tibetan Plateau. Front. Genet. **5:** 4.

Wessinger, C.A. (2021). From pollen dispersal to plant diversification: Genetic consequences of pollination mode. New Phytol. **229:** 3125–3132.

Westerhold, T., Marwan, N., Drury, A.J., Liebrand, D., Agnini, C., Anagnostou, E., Barnet, J.S., Bohaty, S.M., De Vleeschouwer, D., Florindo, F., et al. (2020). An astronomically dated record of Earth's climate and its predictability over the last 66 million years. Science **369** (6509): 1383–1387.

Wilke, C. (2020). ggridges: Ridgeline Plots in 'ggplot2'. R package version 0.5.2. https://wilkelab.org/ggridges/

Xing, Y., and Ree, R.H. (2017). Uplift-driven diversification in the Hengduan Mountains, a temperate biodiversity hotspot. Proc. Natl. Acad. Sci. U.S.A. **114:** E3444–E3451.

Xu, B., Luo, D., Li, Z.M., and Sun, H. (2019). Evolutionary radiations of cushion plants on the Qinghai-Tibet Plateau: Insights from molecular phylogenetic analysis of two subgenera of *Arenaria* and *Thylacospermum* (Caryophyllaceae). Taxon **68:** 1003–1020.

Xu, L., Ou, X., Lai, Z., Zhou, S., Wang, J., and Fu, Y. (2010). Timing and style of Late Pleistocene glaciation in the Queer Shan, northern Hengduan Mountains in the eastern Tibetan Plateau. J. Quat. Sci. **25:** 957–966.

Yang, Z. (2015). The BPP program for species tree estimation and species delimitation. Curr. Zool. **61:** 854–865.

Yang, Z., and Rannala, B. (2010). Bayesian species delimitation using multilocus sequence data. Proc. Natl. Acad. Sci. U.S.A. **107:** 9264–9269.

Zhang, B., Sun, S.F., Luo, W.L., Li, J.X., Fang, Q.E., Zhang, D.G., and Hu, G.X. (2021a). A new brood-pollination mutualism between *Stellera chamaejasme* and flower thrips *Frankliniella intonsa*. BMC Plant Biol. **21:** 562.

Zhang, D.C., Boufford, D.E., Ree, R.H., and Sun, H. (2009). The 29°N latitudinal line: An important division in the Hengduan Mountains, a biodiversity hotspot in southwest China. Nord. J. Bot. **27:** 405–412.

Zhang, J.W., Nie, Z.L., Wen, J., and Sun, H. (2011a). Molecular phylogeny and biogeography of three closely related genera, *Soroseris*, *Stebbinsia*, and *Syncalathium* (Asteraceae, Cichorieae), endemic to the Tibetan Plateau, SW China. Taxon **60:** 15–26.

Zhang, X., Landis, J.B., Sun, Y., Zhang, H., Lin, N., Kuang, T., Huang, X., Deng, T., Wang, H., and Sun, H. (2021b). Macroevolutionary pattern of *Saussurea* (Asteraceae) provides insights into the drivers of radiating diversification. Proc. R. Soc. B Biol. Sci. **288:** 20211575.

Zhang, Y.H., Volis, S., and Sun, H. (2010). Chloroplast phylogeny and phylogeography of *Stellera chamaejasme* on the Qinghai-Tibet Plateau and in adjacent regions. Mol. Phylogenet. Evol. **57:** 1162–1172.

Zhang, Z.Q., Zhang, Y.H., and Sun, H. (2011b). The reproductive biology of *Stellera chamaejasme* (Thymelaeaceae): A self-incompatible weed with specialized flowers. Flora **206:** 567–574.

Zhao, J., Li, S., Farnsworth, A., Valdes, P.J., Reichgelt, T., Chen, L., Zhou, Z., and Su, T. (2022). The Paleogene to Neogene climate evolution and driving factors on the Qinghai-Tibetan Plateau. Sci. China Earth Sci. **65:** 1339–1352.

Zhao, Y.J., Yin, G.S., Pan, Y.Z., Tian, B., and Gong, X. (2021). Climatic refugia and geographical isolation contribute to the speciation and genetic divergence in Himalayan-Hengduan tree Peonies (*Paeonia delavayi* and *Paeonia ludlowii*). Front. Genet. **11:** 595334.

Zheng, B., Xu, Q., and Shen, Y. (2002). The relationship between climate change and Quaternary glacial cycles on the Qinghai-Tibetan Plateau: Review and speculation. Quatern. Int. **97:** 93–101.

Zhou, S.Z., and Li, J.J. (1998). The sequence of Quaternary glaciation in the Bayan Har Mountains. Quatern. Int. **45-46:** 135–142.

Zhou, S.Z., Wang, X.L., Wang, J., and Xu, L.B. (2006). A preliminary study on timing of the oldest Pleistocene glaciation in Qinghai–Tibetan Plateau. Quatern. Int. **154-155:** 44–51.

SUPPORTING INFORMATION

Additional Supporting Information may be found online in the supporting information tab for this article: http://onlinelibrary.wiley.com/doi/10.1111/jipb.13663/suppinfo

Figure S1. Genetic variance as indicated by analysis of molecular variance (AMOVA)-based F_{ST} within the paired population level
Figure S2. Structured cluster for 34 populations of *Stellera chamaejasme*
Figure S3. Distribution of single nucleotide polymorphism (SNPs) along the principal component (PC) of genetic variation
Figure S4. Co-ancestry for the four cryptic species of *Stellera chamaejasme*
Figure S5. Population-level cryptic species-wise maximum likelihood (ML) phylogenetic tree inferred with IQ-TREE
Figure S6. Population-level cryptic species-wise maximum likelihood (ML) phylogenetic tree inferred with IQ-TREE
Figure S7. Bayesian phylogenetic tree inferred with MrBayes
Figure S8. Exploring the Isolation-by-Distance (IBD) effect in *Stellera chamaejasme* through linear regression analysis
Figure S9. Unveiling genetic structures in populations using unsupervised machine learning (UML) clustering analysis
Figure S10. Correlation heatmap of the cryptic species, confirming the least pair correlations across 29 least correlated morphological traits
Figure S11. The ridgeplots (A–A3) visualization for the comparison of all the morphological traits between the four cryptic species of *Stellera chamaejasme*
Figure S12. Phylogenetic traitgrams for significant morphological traits
Figure S13. Deciphering morphological trait contributions and clustering in *Stellera chamaejasme*
Figure S14. Ecological characterization for *Stellera chamaejasme*
Figure S15. Habitat suitability predicted by ensemble species distribution modeling (eSDM) for the cryptic species *Stellera chamaejasme*
Figure S16. Niche dynamics of *Stellera chamaejasme*

Table S1. Restrictions site-associated DNA sequencing (RAD-seq) reads information and quality control statistics for every 251 individuals of *Stellera chamaejasme* and three closely related outgroups
Table S2. Population summary statistics calculated for variant positions of 23,215 restrictions site-associated DNA sequencing (RAD-seq) loci
Table S3. Population summary statistics calculated for all positions of 23,215 restrictions site-associated DNA sequencing (RAD-seq) loci
Table S4. The paired population-level estimation of genetic diversity indices, Φ_{ST} means (lower left diagonal) and F_{ST}' means (upper right diagonal) for 34 populations estimated using the populations pipeline in *Stacks*
Table S5. The paired mean absolute differentiation (D_{XY}) among 34 populations estimated using the populations pipeline in *Stacks*
Table S6. The population-level cryptic species-wise estimation of the genetic diversity indices; Φ_{ST} means, D_{XY} means, and F_{ST}' means
Table S7. Comparison among the nucleotides substitution model for the selection of best fitting model based on Akaike information criterion (AIC), Bayesian information criterion (BIC), and corrected AIC (AICc) measurements using Modeltest-NG

Table S8. Impact of the prior specification on the number of delimited cryptic species using Bayesian phylogeny and phylogeography (BPP) analysis (A11 = joint species delimitation and species tree estimation). Posterior probability values (P) are averaged over two runs

Table S9. Marginal likelihood estimates under different scenarios (N, A1, A2, A3, A4) from Path Sampler analysis for BFD* (Bayes Factor Delimitation, *with genomic data) in 251 individuals and three closely related taxa (*Daphne tangutica*, *Daphne holosericea*, *Wikstroemia ligustrina*)

Table S10. Descriptive statistics (mean ± *SE*) and their Shapiro-Wilk normality test for the normal distribution of the continuous and categorical morphological traits for four cryptic species of *Stellera chamaejasme* observed from the herbarium specimens

Table S11. Levene's test of homogeneity of variance assumptions for the morphological traits of *Stellera chamaejasme*

Table S12. Multivariate analysis of variance (MANOVA) test for the significant differences between four cryptic species of *Stellera chamaejasme* for continuous morphological traits and the trait-wise test of significant difference between the cryptic species

Table S13. *Post hoc* Tukey's Honestly Significant Difference (HSD) multivariate analysis of variance (MANOVA) test for the trait-species-wise significance difference between the four cryptic species of *Stellera chamaejasme*

Table S14. Predictive variable selection for the ensemble species distribution modeling (eSDM) of each cryptic species of *Stellera chamaejasme*

Table S15. Variance inflation factor (VIF) in different test runs to select explanatory variables for four cryptic species of *Stellera chamaejasme*. VIF <10 (bold text) are the selected predictive variables

Table S16. Consensus land-cover selection for each cryptic species of *Stellera chamaejasme* based on the presence of the number of occurrence records

Table S17. Model evaluation indices for the ensemble species distribution modeling (eSDM) of each cryptic species of *Stellera chamaejasme* using *Biomod2* in R-programming language

Scan using WeChat with your smartphone to view JIPB online

Scan with iPhone or iPad to view JIPB on Twitter